Liquid-Metal-Based Nanophotonic Structures for High-Performance SEIRA Sensing

Xianglong Miao, Ting Shan Luk and Peter Q. Liu\*

X. Miao, P. Q. Liu

Department of Electrical Engineering, University at Buffalo, The State University of New

York, Buffalo, New York 14260, United States

\*E-mail: pgliu@buffalo.edu

T. S. Luk

Center for Integrated Nanotechnologies, Sandia National Laboratories, Albuquerque, New

Mexico 87123, USA

Keywords: SEIRA, sensor, liquid metal, liquid gallium, nanophotonics

Surface-enhanced infrared absorption (SEIRA) spectroscopy can provide label-free, non-

destructive detection and identification of analytes with high sensitivity and specificity, and

therefore has been widely used for various sensing applications. SEIRA sensors usually employ

resonant nanophotonic structures, which can substantially enhance electric field and hence

light-matter interactions by orders of magnitude in certain nanoscale hot spots of the devices.

However, as ever smaller hot spots are employed to further enhance the field, the delivery of

analytes into such hot spots becomes increasingly challenging. Here, we demonstrate high-

performance nanophotonic SEIRA sensors based on nano-patch antennas with a liquid gallium

ground plane, which not only lead to ultra-high field confinement and enhancement, but also

allow for convenient and efficient delivery of analytes into nanometric hot spots by employing

a simple procedure suitable for point-of-care applications. Our sensors exhibited superior

sensitivity in the mid-infrared spectral region. Around 10% molecular vibrational signals (i.e.,

the modulation of a sensor's reflection spectrum owing to the molecular vibrational modes of

the analytes) near 2900 cm<sup>-1</sup> were achieved from sensing monolayer 1-octadecanethiol. Our

cost-effective and reliable method for realizing liquid-metal-based nanophotonic structures

provides a new strategy for developing high-performance sensors and other photonics

applications in the infrared region.

1

#### 1. Introduction

Molecular vibrations can interact with and absorb infrared light to produce fingerprint-like spectra, which have been exploited for label-free, non-destructive detection and identification of specimens with the help of infrared absorption spectroscopy.<sup>[1]</sup> However, typical molecular vibrational absorption is relatively weak and difficult to detect when the amount of analyte is low, which limits its widespread use in a variety of sensing applications. As molecular vibrational absorption is generally proportional to the intensity of electric field experienced by the molecules,<sup>[2]</sup> SEIRA sensors based on a variety of resonant nanophotonic structures have been demonstrated to significantly enhance molecular vibrational absorption and consequently achieve high sensitivity performance.<sup>[3]</sup>

Resonant nanophotonic structures excited by incident light can confine highly enhanced electric field in deep-subwavelength regions, known as "hot spots", in which the interactions between light and analyte molecules can be drastically enhanced, leading to significant improvement of the sensing performance. Designing nanophotonic structures with smaller hot spots is a widely utilized strategy to increase field enhancement and improve sensor performance. A variety of nanophotonic structures with nanometric gaps have been demonstrated for sensing applications, such as dimer antennas, [4, 5] split-ring resonators, [6] coaxial disk resonators, [7, 8] and nano-patch antennas. [9-11] However, with the gap size decreasing down to the nanometric scale, it becomes increasingly difficult to deliver analyte molecules into these gaps (i.e., the hot spots), especially when the gap size is comparable to typical sizes of molecules. This issue fundamentally limits the further performance improvement of nanophotonic sensors. An effective approach to addressing this issue is to deliver the analytes before forming the nanometric gaps (or other types of hot spot structures). For example, metallic nanoparticles coated with analyte thin films can form super-crystals with nanometric separation gaps. [12, 13] In a recent study, such supercrystals of gold nanoparticles coated with thiolated polystyrene molecules were demonstrated

to function as SEIRA sensors for sensing the polystyrene molecules with high performance.<sup>[13]</sup> Another previous demonstration of SEIRA sensors based on graphene acoustic plasmon resonators realized effective delivery of analytes into nanometric gaps by first spin-coating a thin analyte film on gold nanoribbons, and subsequently transferring graphene onto the analyte film, which led to the successful detection of SEIRA signals from sub-nm thick analyte films.<sup>[14]</sup> Nevertheless, assembling super-crystals of metal nanoparticles or transferring graphene to form the complete sensor structures is not a simple and straightforward process, and hence may not be suitable for point-of-care applications.

Here, we show that employing liquid metals, such as liquid gallium, is a convenient and effective approach to realizing high-performance SEIRA sensors with nanometric gaps filled with analyte molecules. As a proof-of-concept demonstration, we developed a SEIRA sensor structure consisting of an array of metallic nanostrips separated by a nanometric dielectric layer from a metallic ground plane, which were essentially an array of nano-patch antennas. [15] The nanometric dielectric layer was the sensing target, i.e., a thin film of analyte molecules, which was coated on the metallic nanostrips via physical/chemical adsorption or spin-coating. Subsequently, liquid gallium was added to cover the thin film of analyte molecules and function as the ground plane of the nano-patch antennas. Thanks to the highly confined and enhanced electric field in the nanometric gaps between the metallic nanostrips and the liquid gallium, the molecular vibrational signals associated with the analyte film can be substantially enhanced. These SEIRA sensors exhibited state-of-the-art sensing performance for nanometric analyte thin films, such as monolayer 1-octadecanethiol (ODT). Our experimental results also indicate that the liquid gallium did not cause damage to or change the properties of the analyte films. In addition, the liquid gallium can be conveniently removed completely from the sensor surface after a measurement, which makes it easy to reuse such sensors. This work demonstrates several key advantages of using liquid gallium for SEIRA sensing applications, and also points toward other potential applications of liquid metals in a variety of photonic structures and devices operating in the infrared spectral region.

#### 2. Results and Discussion

#### 2.1. Sensor Design

Figure 1a shows the schematic of our SEIRA sensor design employing a nano-patch antenna structure. The thin analyte film is sandwiched between patterned gold nanostrips and a metallic ground plane. Rather than using a conventional noble metal such as gold or silver, liquid gallium is employed to form the ground plane, which has several key advantages. First of all, the fluidic nature of liquid gallium allows it to be straightforwardly spread on the analyte film and form the nano-patch antenna structures, without the need for any bulky equipment such as a metal evaporator. Such a sensor design and preparation procedure also make the delivery of analytes into the nanometric sensing hot spots (i.e., the nanometric gaps) convenient and efficient, as the liquid gallium ground plane is added after the analyte thin film has been introduced onto the gold nanostrips. This is a key advantage over the conventional approach of fabricating the complete sensor structures and then introducing the analytes, as it may be very difficult and time-consuming to deliver analytes into hot spots with nanometric dimensions. Secondly, gallium has a low melting point (~29.7 °C) close to room temperature and hence is convenient to use. In addition, gallium is non-toxic and biocompatible, which are particularly important properties for a variety of biosensing applications. [16, 17] Furthermore, liquid gallium has favorable metal properties for photonics applications, including a relatively high bulk plasma frequency (around 15 eV in terms of energy) and relatively low extrinsic loss thanks to the inherently smooth liquid surface and the absence of grain boundaries.<sup>[18-20]</sup> Taking advantage of such material properties, liquid gallium has previously been exploited for plasmonics applications in the visible spectral region [16-18] as well as for terahertz photonics.[21-

<sup>23]</sup> Nevertheless, potential applications of liquid gallium for mid-infrared photonics have largely not been explored.

We measured the permittivity function of liquid gallium across a wide infrared spectral region using spectroscopic ellipsometry, and the results are shown in **Figure 1b-c**. The large absolute values of its permittivity function indicates that liquid gallium behaves as a good metal in this spectral region. Based on the experimental permittivity data, we performed full-wave simulation of the designed nano-patch antenna structures with a liquid gallium ground plane. **Figure 1d** shows that such nanophotonic structures can indeed achieve ultra-high confinement and enhancement of electric field intensity in the nanometric gaps (by about 3 orders of magnitude), which in turn can lead to large enhancement of SEIRA signals associated with the molecular vibrational absorption from the analytes located in these gaps. In addition, such nanopatch antenna structures allow for nearly perfect spatial overlap between an analyte thin film coated on the gold nanostrips and the highly enhanced electric field. Therefore, the presented sensor designs are especially suitable for sensing analytes in the form of continuous nanometric thin films.

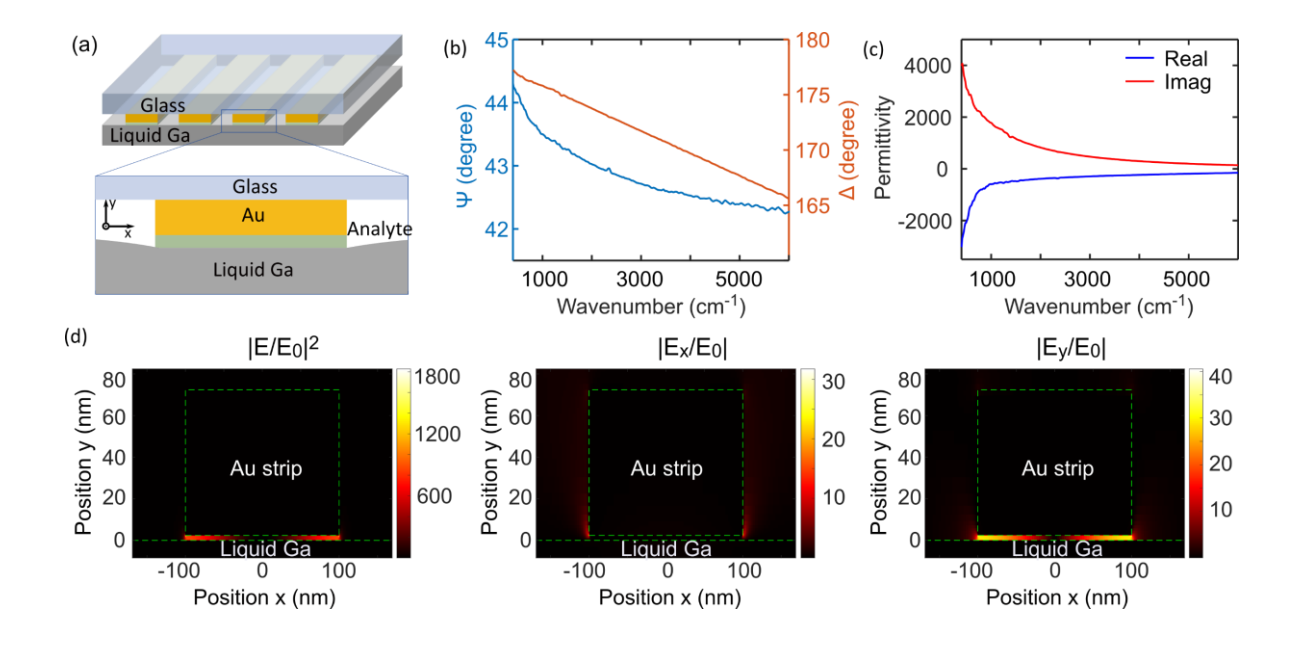
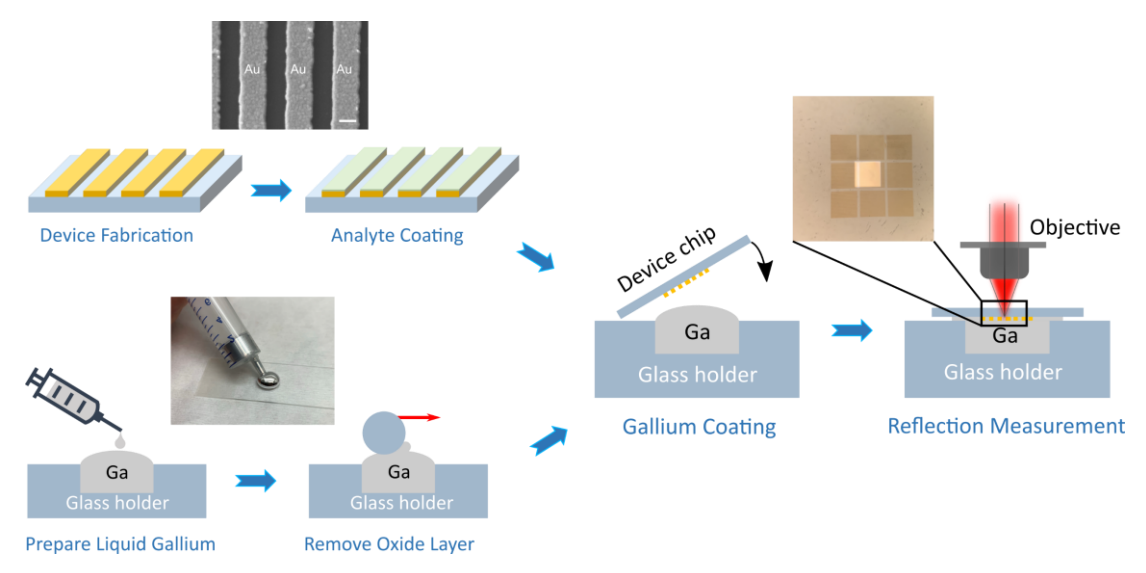


Figure 1. Structure of liquid-gallium-based SEIRA sensors. (a) Schematic of the sensor structure. (b) Measured spectra of the ellipsometry parameters  $\Psi$  and  $\Delta$  for a flat liquid gallium surface, where  $\Psi$  and  $\Delta$  are related to the complex reflectance ratio as  $r_p/r_s = \tan \Psi \cdot e^{i\Delta}$ ,  $r_p$  and  $r_s$  are the complex reflectance for the p-polarization and s-polarization, respectively. (c) The real part (blue line) and imaginary part (red line) of the relative permittivity function of liquid gallium calculated from the ellipsometry measurement results in (b). (d) Simulated distributions of the electric field intensity (left panel), the amplitude of the x-component of the electric field (middle panel), and the amplitude of the y-component of the electric field (right panel), at the resonance of the nano-patch antenna employing a liquid gallium ground plane. These field distributions are all normalized to the incident field.

#### 2.2. Procedure for Preparing Liquid-Gallium-Based Sensors

**Figure 2** schematically shows the preparation procedure of our sensors. Sensor chips consisting of arrays of gold nanostrips on a glass or calcium fluoride (CaF<sub>2</sub>) substrate were fabricated with electron-beam lithography for patterning, followed by the deposition of a 70 nm thick gold film and a lift-off process (see "**Methods**"). Then the analyte molecules were coated on the surface of the gold nanostrips with methods such as physical/chemical adsorption or spin-coating, which are widely used methods for introducing analytes onto nanophotonic sensors. [14, 24, 25] Solid gallium in a syringe was melted by slightly warming up the syringe on a hot plate to above 30 °C, and then a small amount of liquid gallium (about 0.1 mL) was injected into a glass holder. Although room temperature is slightly lower than the melting point of liquid gallium, it is not necessary to provide continuous heating because the liquid gallium can maintain its liquid phase even at temperatures significantly below its melting point thanks to the super-cooling effect. [26] Liquid gallium exposed to air has a thin oxide layer on the surface, which can be peeled off by simply scraping the liquid gallium surface with a thin plastic rod. After removing

the oxide layer, the sensor chip coated with the analyte thin film were immediately placed on the liquid gallium to form the complete nano-patch antenna structures. A flat and mirror-like liquid gallium surface was usually observed, which indicated the formation of a good contact interface between the liquid gallium and the sensor chip. Subsequently, the infrared reflection spectra of the complete nano-patch antenna structures were measured with the light incident from the transparent substrate side of the sensor (see Figure 2). Compared with the conventional methods of depositing solid noble metals, such as evaporation or sputtering, this method of coating liquid metal to complete the sensor structures is simple and quick to operate, and it does not require expensive and bulky equipment, which significantly reduces the cost and is suitable for point-of-care sensing applications.



**Figure 2.** Schematics of the procedure for preparing liquid-gallium-based SEIRA sensors for sensing nanometric analyte films. An SEM image of the fabricated gold nanostrips, a photo of a small quantity of liquid gallium squeezed out of a syringe and onto a glass slide, and an optical image of a sensor chip observed under the microscope are also shown in the figure.

#### 2.3. Sensing of Monolayer ODT

For a proof-of-concept demonstration of the sensor's performance, we chose ODT as the model

analyte. ODT is one of the alkanethiols which can form a self-assembled monolayer (SAM) with a thickness of ~2.4 nm on gold surface. The permittivity of SAM ODT was extracted from experimental data (see Supporting Information S1) and is shown in Figure 3a. ODT has four vibrational modes around 2900 cm<sup>-1</sup>, which correspond to the symmetric and anti-symmetric stretching vibrations of CH<sub>2</sub>- and CH<sub>3</sub>- groups, respectively. [27] Multiple arrays of gold nanostrips with widths ranging from 200 nm to 400 nm were fabricated, so that the resonances of the corresponding nano-patch antennas can cover a wide spectral range that contains the ODT vibrational modes. The thickness of the gold nanostrips was 70 nm, and the duty cycle of all the gold nanostrip arrays was 50%. These design parameters were chosen to balance the optimization of the SEIRA sensing performance and the device fabrication reliability. To form the SAM ODT on the surfaces of the gold nanostrips, the sensor chips were immersed in 1 mM ethanol-based ODT solution overnight. After the sensor chips were taken out of the ODT solution, they were thoroughly rinsed with ethanol to remove any unbound ODT molecules and blown dry. Subsequently, the sensor chips were placed on liquid gallium to form the complete sensor structures before the spectroscopic measurement, as shown by the schematic in Figure **3b**. Our experimental observations indicated that this sample preparation procedure can reliably form SAM ODT that completely covers the gold surface. If the SAM ODT did not completely cover the gold surface, the liquid gallium would make direct contact with and "erode" the exposed regions of the gold surface, which was rarely observed in our experiments. The fact that the formation of SAM ODT on gold surface is a relatively reliable process also suggests that the performances of our sensors and the different SEIRA sensors reported in the literature for sensing SAM ODT can be directly compared.

The measured reflection spectra of the sensors with varied gold nanostrip widths are shown in **Figure 3c**. The incident light was linearly polarized perpendicular to the gold nanostrips. The different sensors exhibited resonances (i.e., the reflection dips in Figure 3c) covering a wide

spectral range, from ~2800 cm<sup>-1</sup> to ~4900 cm<sup>-1</sup>, as the width of the gold nanostrips varied from 400 nm to 240 nm. As highlighted by the yellow region in Figure 3c, the molecular vibrational modes of the SAM ODT near 2900 cm<sup>-1</sup> coupled to the resonances of the sensors, which resulted in significant modulations of the reflection spectra in this spectral region. In addition, such molecular vibrational signals (i.e., the modulation of the sensors' reflection spectra) associated with the SAM ODT became much stronger when the resonant frequency of the sensor structure matched the ODT vibrational modes, since the highest electric field intensity confined in the nanometric gaps occurs near the resonant frequencies of these nano-patch antenna structures. To further analyze these spectral features due to the analyte, we extracted the net molecular vibrational signals (i.e. the SEIRA signals) by performing a baseline subtraction [28] and the results are plotted in Figure 3d. Individual spectral features associated with the aforementioned four ODT vibrational modes, highlighted by the colored regions in Figure 3d, can be clearly observed in these spectra. The maximum molecular vibrational signal achieved was approximately 10%, which was obtained from the sensor with 400 nm wide gold nanostrips, as its resonance matched the ODT vibrational modes the best. Such a sensing performance is superior to those of the previous demonstrations of SEIRA sensing of SAM ODT. [6, 9, 27, 29-31] In addition to the large field enhancement in the nanometric gaps and the high spatial overlap between the monolayer ODT and the enhanced field thanks to the liquid gallium ground plane, the geometry of the elongated nanostrips also contributes to improving the SEIRA sensing performance as it makes efficient use of the device surface area. The spectral features associated with the ODT vibrational modes exhibited asymmetric Fano-like line shapes, which is a result of the interference between the broadband resonance of the nano-patch antenna structure and the relatively narrow vibrational modes of ODT.<sup>[32]</sup> We also simulated and experimentally characterized the reflection spectra of the devices with the incident light linearly polarized parallel to the gold nanostrips, and the corresponding results are shown in Figure S2 in the Supporting Information. Since these nano-patch antennas do not have resonant modes in the

spectral region of interest for this polarization of incident light (see Figure S2a), as expected, no significant SEIRA signal was observed (see Figure S2c).

After the optical measurement, the liquid gallium can be conveniently removed from the sensor surface by simply lifting the sensor chip up. As liquid gallium generally does not wet with organic materials, and the surface tension of liquid gallium is relatively large (around 708 mN/m), [33] it can be easily removed from the thin analyte film without leaving residual. We imaged the sensor chip surface after removing the liquid gallium with a scanning electron microscope (SEM) (see **Figure 3e**). The gold nanostrips appeared to be the same as before they were contacted with liquid gallium, and there was no evident gallium residual on the chip surface (see the zoomed-in image). We also characterized the sensor surface with energy-dispersive X-ray spectroscopy (EDS) (see **Figure 3f**) to further examine whether there was any gallium residual. No gallium peak was found in the EDS spectra, which indicated that the sample was not contaminated by Ga. Removing the liquid gallium without residual allows for other subsequent analysis of the analytes and makes our sensor chips reusable (since many types of analytes can also be thoroughly removed), which can further reduce the cost of the various potential sensing applications enabled by such devices.

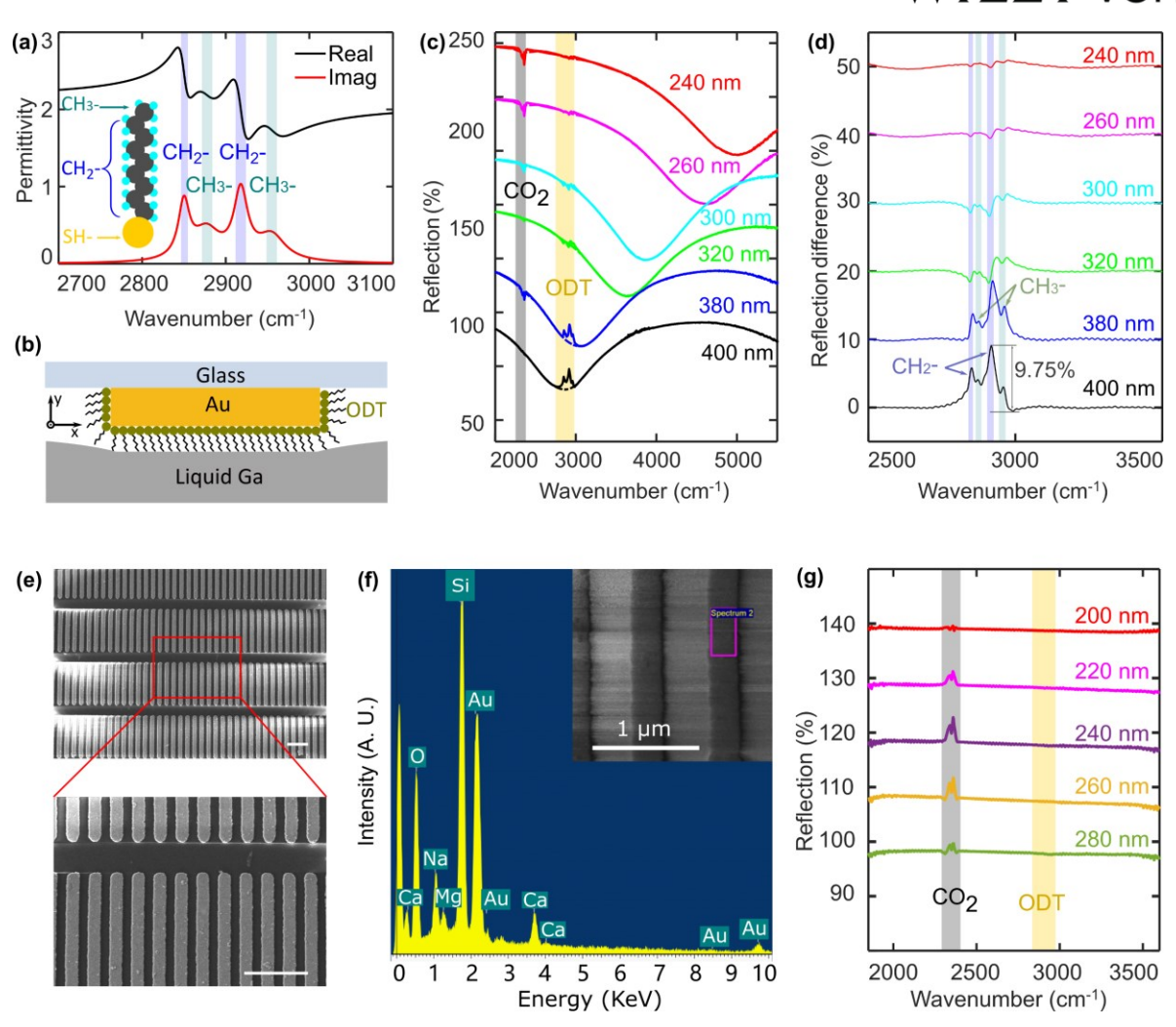


Figure 3. Experimental results of sensing SAM ODT. (a) Relative permittivity of ODT extracted from the measured reflection spectrum of SAM ODT on a flat gold surface. The purple and green shaded regions mark the CH<sub>2</sub>- and CH<sub>3</sub>- vibrational modes. The inset gives a schematic of the ODT molecule. (b) Schematic of a nano-patch antenna with the SAM ODT sandwiched between the gold nanostrip and the liquid gallium ground plane. (c) Measured reflection spectra of liquid-gallium-based sensors with SAM ODT. The yellow shaded region highlights the spectral range containing the ODT molecular vibrational modes. The absorption lines near 2400 cm<sup>-1</sup> are due to CO<sub>2</sub> absorption in the optical path of our experimental setup. The spectra plotted in (c) are stacked vertically with 25% offset between neighboring curves. (d) Extracted net molecular vibrational signals associated with the SAM ODT from (c). The spectra plotted in (d) are stacked vertically with 10% offset between neighboring curves. (e) SEM images of a sensor surface after the liquid gallium was removed. The scale bars are both

2  $\mu$ m. (f) Measured EDS spectrum of the gold nanostrip surface after the liquid gallium was removed. The electron gun accelerating voltage was 20 kV. The inset is an SEM image of the device surface and the EDS measurement region is marked by the pink rectangle. The gallium peak ( $K\alpha - 9.241 \text{ keV}$ ) is not observed in the EDS spectrum. (g) Measured reflection spectra of the sensors with a gold ground plane directly deposited on the SAM ODT using electron-beam evaporation. The spectra plotted in (g) are stacked vertically with 10% offset between neighboring curves.

To compare the sensing performance of our liquid-gallium-based nano-patch antenna sensors to similar devices with a conventional ground plane made of noble metals, we fabricated several reference devices with a deposited gold or silver film as the ground plane. We found that when the gold or silver film was deposited directly on the SAM ODT using an electron-beam evaporator, neither the expected nano-patch antenna resonance nor the ODT absorption peaks were observed in the measured reflection spectra (see Figure 3g). Note that the same ODT solution and SAM ODT preparation procedure were used for all the samples, and our repeated tests confirmed that the sample preparation procedure can reliably form SAM ODT that completely covers gold surface. Therefore, the quality of the SAM ODT on all the devices should be similar before either the liquid gallium or the deposited metal or dielectric film was added. The results in Figure 3g suggest that the SAM ODT was likely damaged during the metal deposition and consequently the nano-patch antenna structures were not successfully formed, because any direct contact between a gold nanostrip and the metallic ground plane establishes a "short circuit" that may severely quench the nano-patch antenna resonance. This issue associated with the metal deposition further demonstrates the advantage of using liquid gallium to form the ground plane. To protect the SAM ODT from the metal deposition process, we prepared additional reference devices and deposited a thin aluminum oxide layer on the SAM ODT with atomic layer deposition (at 80 °C), before depositing the gold ground plane with the electron-beam evaporator. The reflection spectra of the best reference devices (with ~3 nm

aluminum oxide) are plotted in Figure S3c in the Supporting Information, which exhibit both the nano-patch antenna resonances and the SEIRA signals associated with the ODT vibrational modes. The net SEIRA signals due to the ODT vibrational modes are extracted and plotted in Figure S3d in the Supporting Information. Compared to the results from the liquid-galliumbased sensors, the maximum SEIRA signal obtained with these reference sensors is slightly lower (around 9%), and the signals associated with the CH<sub>3</sub>- vibrational modes are evidently weaker and not clearly resolved. Since the CH<sub>3</sub>- group is located at the end of the carbon-chain in an ODT molecule and constitutes the top surface of the SAM ODT, the weaker signals associated with the CH<sub>3</sub>- vibrational modes suggest that the SAM ODT may still be affected by the depositions of the aluminum oxide film and/or the metal film. In addition, the reference devices with a thinner oxide film showed worse sensing performance (see Supporting Information Figure S3a), likely due to insufficient protection of the SAM ODT. On the other hand, the reference devices with a thicker oxide film also showed lower SEIRA sensing performance, likely owing to the reduced field enhancement in the gap (see Supporting Information Figure S3e). Although adding the oxide layer can protect the analytes, it makes the sensor preparation even more complex and costly, and inevitably increases the gap size of the nano-patch antenna, which in turn decreases the field enhancement and reduces the sensor performance. In comparison, our liquid-gallium-based sensor structures not only allow for simple and cost-effective device fabrication, but also lead to superior field enhancement and sensitivity performance.

#### 2.4. Device Simulation

We also conducted full-wave simulation using the finite-difference time-domain (FDTD) method (see "**Methods**") to further analyze the experimental results and the sensor performance. In our simulation, the thickness of the SAM ODT was set to be 2.4 nm, and the permittivity functions of ODT and liquid gallium were extracted from our experimental characterizations.

Figure 4a shows the simulated reflection spectra of the sensors with the gold nanostrip width ranging from 200 nm to 380 nm. Compared with the experimental results, the simulated reflection spectra have similar spectral features but also exhibit two important discrepancies. First, for the same nanostrip width, the simulated reflection spectrum of a nano-patch antenna array shows a significantly lower resonant frequency than that obtained from the experiment. Second, the simulated molecular vibrational signals caused by the SAM ODT can reach  $\sim 20\%$ , which is about twice as large as those extracted from the experimental spectra. Considering that the non-local effect may play a role in determining the spectral responses of our sensor structures with nanometric gaps, [34] we performed simulation to quantify the influence of the non-local effect (see Supporting Information S4.1 for details). Figure 4b compares the simulated nano-patch antenna resonant frequency, with or without accounting for the non-local effect, to the experimental values (plotted as functions of the inverse of the nanostrip width). Although the simulated resonant frequencies show a small blue-shift when the non-local effect is taken into account, they are still significantly below the corresponding experimental values. Therefore, the non-local effect cannot explain this discrepancy in resonant frequency. Besides the non-local effect, the gap size of the nano-patch antenna may also significantly influence the resonant frequency. As shown in Figure 4c, we simulated the reflection spectra of a nano-patch antenna structure with varied gap sizes (the nanostrip width was fixed at 380 nm). When the gap size is relatively large (e.g., larger than 30 nm), the resonant frequency of the nano-patch antenna shows a relatively weak dependence on the gap size. However, when the gap size becomes smaller, the resonant frequency of the nano-patch antenna exhibits a strong dependence on the gap size, especially when the gap size is below 10 nm. The reflection dip at the resonance also reduces with the decrease of the gap size, as the system deviates further from the critical coupling condition.<sup>[32]</sup> Considering the surface roughness of the gold nanostrips and the relatively large surface tension of liquid gallium, we surmise that the liquid gallium did not form a perfectly conformal contact with the SAM ODT coated on the gold nanostrips. Instead,

owing to the surface roughness of the gold nanostrips, there were randomly distributed small gaps between the liquid gallium and the SAM ODT, which effectively increased the average gap size of the nano-patch antennas and hence led to a significant increase of the resonant frequency.

We characterized the surface morphology of the ODT-covered gold nanostrips using atomic force microscopy (AFM) and found that the surface indeed has randomly distributed protrusions that are several nm in height (see Figure 4d). We further conducted simulations which took into account such surface roughness of the gold nanostrips as well as the corresponding undulating surface profile of the liquid gallium. In the simulation models, the liquid gallium only contacted the protrusions of the SAM ODT-covered rough surface of the gold nanostrips and therefore small air gaps were formed in between the protrusions (see Supporting Information S4.2 for details). Figure 4e compares the experimental spectrum with the simulated spectra obtained with or without taking into account the surface roughness of the gold nanostrips. Indeed, with the surface roughness incorporated in the model, the simulated reflection spectrum significantly shifts to a higher frequency and matches the experimental result well. Since a larger effective gap size results in lower field confinement and enhancement, which in turn reduces the sensor sensitivity, our experimentally demonstrated sensor performance may be further improved significantly by reducing the surface roughness of the gold nanostrips (see Figure S5 in the Supporting Information). This can be achieved, for example, by optimizing the metal deposition process or employing the template stripping method.[35]

#### WILEY-VCH (a) (d) **(b)** 5000 8.3 nm Experiment Wavenumber (cm<sup>-1</sup>) 0000 0000 0000 360 nm Nonlocal Local 340 nm 250 300 nm 200 -7.4 nm Reflection (%) 280 nm 3 3.5 1/w (µm<sup>-1</sup>) 60.0 nm 2.5 4.5 150 (c) 50 **(e)** 100 8.0 40 Gap size (nm) Reflection (%) 80 240 nm 0.6 100 30 0.4 200 nm 20 60 Exp 0.2 50 10 Simu rough Simu smooth 40 3000 4000 2000 3000 4000 2000 2000 3000 4000 5000 6000 Wavenumber (cm<sup>-1</sup>) Wavenumber (cm<sup>-1</sup>) Wavenumber (cm<sup>-1</sup>)

**Figure 4.** Simulation results of the liquid-gallium-based sensors. (a) Simulated reflection spectra of liquid-gallium-based sensors with a 2.4 nm thick (monolayer) ODT in the gaps of the nano-patch antennas. The spectra plotted in (a) are stacked vertically with 25% offset between neighboring curves. (b) Measured and simulated resonant frequencies of the nano-patch antennas versus the inverse of gold nanostrip width. (c) Simulated reflection spectra of the liquid-gallium-based nano-patch antennas with different gap sizes. In the corresponding simulation models, the nanometric gaps of the nano-patch antennas were filled with a dielectric material with a refractive index of 1.45. (d) AFM map of a gold nanostrip surface coated with SAM ODT. (e) Comparison of the experimental reflection spectrum of a sensor to the simulated reflection spectra with smooth or rough gold nanostrip surface. The nanostrip width of this sensor is 380 nm.

#### 2.5. Discussion

Although we utilized SAM ODT as the model analyte to achieve a proof-of-concept demonstration of liquid-gallium-based nanophotonic SEIRA sensors targeting the mid-infrared spectral region around 3000 cm<sup>-1</sup>, this unconventional device architecture and design strategy can be applied to SEIRA sensors targeting other analytes and other infrared spectral regions,

since liquid gallium exhibits the properties of a good metal across a broad infrared spectral range (Figure 1c). To demonstrate the spectral versatility of such liquid-gallium-based nanophotonic sensors, we also implemented another batch of sensors by simply scaling up the structure dimensions to target the spectral region around 1500 cm<sup>-1</sup>, which is of crucial importance for various biosensing applications because it contains the amide bands of proteins.<sup>[24,25]</sup> In this case, we chose poly(methyl methacrylate) (PMMA) as the model analyte to demonstrate the sensor performance, as PMMA has multiple vibrational modes in this spectral region and can be conveniently spin-coated on the surface of the gold strips (see "Methods"). These sensors also demonstrated high sensing performance for PMMA thin films of varied thicknesses (see Supporting Information S5 for details), even though the device structures were not systematically optimized.

In addition to gallium, several other pure metals are also in the liquid phase at moderate temperatures, such as the alkali metals (e.g., potassium, rubidium) and mercury, which in principle can be used for realizing liquid-metal-based nanophotonic structures and devices. However, alkali metals have high chemical reactivity and high costs, whereas mercury has severe toxicity, and therefore they are not suitable for sensing applications. In this perspective, liquid gallium has a unique advantage. Furthermore, several gallium-based alloys, such as the eutectic gallium-indium and galinstan, have even lower melting points and are also cost-effective, making them candidate liquid metals for realizing the demonstrated nanophotonic SEIRA sensors which are suitable for point-of-care applications.

#### 3. Conclusion

In conclusion, we experimentally demonstrated high-performance SEIRA sensors based on nano-patch antenna structures which employ liquid gallium as the ground plane. Thin analyte films can be conveniently coated on patterned gold nanostrips and then covered by liquid gallium to form the complete nano-patch antenna structures with nanometric gaps, in which ultra-high field intensity is confined. Therefore, this approach achieves both sensing hot spots with exceedingly large field enhancement and efficient delivery of analytes into the hot spots without affecting the properties of the analytes, leading to high-performance SEIRA sensing of nanometric analyte films. A simple and effective procedure was developed to cover the sensor chips with liquid gallium for optical measurement, and to remove the liquid gallium afterwards which allows the sensor chips to be reused. Our liquid-gallium-based SEIRA sensors produced around 10% molecular vibrational signals near 2900 cm<sup>-1</sup> from SAM ODT, which is a performance superior to those of the previous demonstrations of SEIRA sensing of SAM ODT in the literature [6, 9, 27, 29-31] and our reference sensors employing a noble metal ground plane. We also demonstrated sensors which targeted the spectral region near 1500 cm<sup>-1</sup> and achieved high-performance sensing of nanometric PMMA films. In-depth comparison and analysis of our experimental and simulation results further suggest that the sensing performance of our liquid-gallium-based sensors can be further improved by reducing the surface roughness of the patterned gold nanostrips, which currently limits the minimum effective gap size of the nanopatch antenna structures. The demonstrated cost-effective and reproducible method of employing liquid metals to construct nanophotonic structures with ultra-high field confinement and enhancement provides a new platform for various molecular sensing applications, and may also be used for enhancing other types of light-matter interactions for a broad range of applications, such as index sensing, surface-enhanced Raman scattering sensing, nonlinear optics and cavity quantum electrodynamics.

#### 4. Methods

*Numerical simulation*: Numerical simulations were conducted by using a commercial software (Lumerical FDTD Solutions) which is based on the FDTD method. Two-dimensional

simulations were performed with periodic boundary conditions in the device plane and perfectly matched layer (PML) boundary conditions along the light propagation direction. The relative permittivity of ODT and liquid gallium were derived from the experimental results. The relative permittivity of gold was obtained from tabulated data. [36] The thickness of the SAM ODT is set to 2.4 nm. The plane wave source and the reflection monitor were positioned at 5  $\mu$ m and 7  $\mu$ m above the gold nanostrip, respectively. The mesh size in the nanometric gap (i.e., the SAM ODT layer) was 0.3 nm. Three-dimensional simulations were performed to account for the surface roughness of the gold nanostrips (see S4.2 in the Supporting Information for details).

Device fabrication: The substrates (glass coverslips or CaF2 substrates) were cleaned with acetone/isopropyl alcohol (IPA) in an ultrasonic bath, followed by oxygen plasma cleaning. A 10 nm thick Ge film was then deposited on the substrate using an electron-beam evaporator to provide a conductive layer, so that the charging effect can be mitigated during the subsequent electron-beam lithography step. A bi-layer electron-beam lithography resist consisting of a ~250 nm thick bottom layer of copolymer (MicroChem MMA (8.5) MAA EL 9) and a ~70 nm thick top layer of PMMA (molecular weight 950K, MicroChem 950 PMMA A2) were spin-coated on the substrate surface, followed by baking on a hot plate at 180 °C for 2 minutes. Nanostrip arrays were patterned using electron-beam lithography at a 100 kV accelerating voltage, 2 nA beam current, and 800  $\mu$ C/cm² exposure dose. The samples were immersed in a mixture of methyl isobutyl ketone and IPA (1:3) at room temperature for 45 seconds to develop the lithography patterns. Subsequently, 2 nm Ti and 70 nm gold were deposited on the sample surface using the electron-beam evaporator, followed by a metal lift-off process in acetone to form the gold nanostrip arrays.

Formation of SAM ODT on gold nanostrips: An ODT solution at a concentration of 1 mM was prepared by adding 86 mg ODT into 300 mL ethanol. The fabricated sensor chips were first

cleaned in hydrochloric acid for 2 mins to remove ionic and metallic contaminations on the gold surface, followed by rinsing in deionized water. Then the sensor chips were immersed in acetone and IPA to remove organic residuals. After an oxygen plasma cleaning to further remove organic residuals and modify the surface potential, the sensor chips were immediately immersed in the 1 mM ODT solution for at least 12 hours. Then the sensor chips were taken out of the ODT solution and rinsed in ethanol thoroughly to remove unbound ODT molecules. The ODT molecules form strong S-Au bonds on gold surfaces,<sup>[37]</sup> leading to the formation of SAM ODT that completely covers the surface of the gold nanostrips and is not affected by the process of rinsing with ethanol. In contrast, the ODT molecules on the surface of the substrate or above the SAM ODT are unbound can be easily removed by the ethanol rinsing process.

Spin-coating PMMA thin films and thickness measurement: PMMA solutions with concentrations of 0.5% and 1%, respectively, were prepared by diluting a commercial 2% PMMA in anisole solution (molecular weight 495K, MicroChem 495 PMMA A2). The sensor chips were cleaned and the PMMA solutions of three different concentrations (i.e., 2%, 1% and 0.5%) were added onto the surfaces of different sensor chips, spin-coated at 4000 rpm for 60 s and left in the air to dry, resulting in PMMA thin films of different thicknesses. The thicknesses of the PMMA thin films were measured with an ellipsometer (Film Sense FS-1), and the measurement results were further verified by AFM characterization after removing small portions of the PMMA films with a razor blade.

Spectra measurement: All the reflection spectra of the sensors were measured under ambient condition at room temperature, using a Fourier transform infrared spectrometer (FTIR, Bruker Vertex 70 v) which was connected to an infrared microscope equipped with a liquid nitrogen-cooled mercury-cadmium-telluride detector. The incident broadband infrared light from a Globar inside the FTIR was focused by a reflective Cassegrain objective (NA = 0.58, 15X)

magnification) of the microscope down to a square area of  $\sim 100~\mu m$  by  $100~\mu m$  on the sensor. The reflected light was collected by the same objective. A wire grid polarizer was used to make the incident light polarized perpendicular to the gold nanostrips. The reference reflection spectra were measured from blank regions on the sensor chip (i.e., no gold nanostrips, only a flat liquid gallium surface or a flat gold surface below the substrate). Each spectrum was measured at a spectral resolution of  $4~cm^{-1}$  and averaged over 500~scans.

#### **Supporting Information**

Supporting Information is available from the Wiley Online Library or from the author.

#### Acknowledgments

This work is supported in part by the National Science Foundation (NSF) (Award No. ECCS-1847203), and the Center for Integrated Nanotechnologies, an Office of Science User Facility operated for the U.S. Department of Energy (DOE) Office of Science.

Received: ((will be filled in by the editorial staff))
Revised: ((will be filled in by the editorial staff))
Published online: ((will be filled in by the editorial staff))

#### References

- [1] F. Neubrech, C. Huck, K. Weber, A. Pucci, H. Giessen, *Chem. Rev.* **2017**, 117, 5110.
- [2] J. F. O'Hara, R. Singh, I. Brener, E. Smirnova, J. Han, A. J. Taylor, W. Zhang, *Opt. Express* **2016**, 16, 1786.
- [3] A. Hartstein, J. R. Kirtley, J. C. Tsang, *Phys. Rev. Lett.* **1980**, 45, 201.
- [4] C. Huck, F. Neubrech, J. Vogt, A. Toma, D. Gerbert, J. Katzmann, T. Hartling, A. Pucci, *ACS Nano* **2014**, 8, 4908.
- [5] L. Dong, X. Yang, C. Zhang, B. Cerjan, L. Zhou, M. L. Tseng, Y. Zhang, A. Alabastri, P. Nordlander, N. J. Halas, *Nano Lett.* **2017**, 17, 5768.
- [6] E. Cubukcu, S. Zhang, Y.-S. Park, G. Bartal, X. Zhang, Appl. Phys. Lett. 2009, 95, 043113.

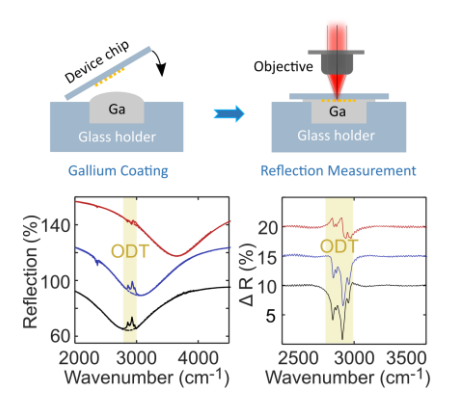
- [7] D. Yoo, D. A. Mohr, F. Vidal-Codina, A. John-Herpin, M. Jo, S. Kim, J. Matson, J. D. Caldwell, H. Jeon, N. C. Nguyen, L. Martin-Moreno, J. Peraire, H. Altug, S.-H. Oh, *Nano Lett.* **2018**, 18, 1930.
- [8] X. Miao, G. Li, L. Xiao, P. Q. Liu, ACS Appl. Nano Mater. 2019, 2, 6798.
- [9] I. Hwang, J. Yu, J. Lee, J.-H. Choi, D.-G. Choi, S. Jeon, J. Lee, J.-Y. Jung, *ACS Photonics* **2018**, 5, 3492.
- [10] T. H. H. Le, A. Morita, K. Mawatari, T. Kitamori, T. Tanaka, ACS Photonics 2018, 5, 3179.
- [11] X. Miao, L. Yan, Y. Wu, P. Q. Liu, Light Sci. Appl. 2021, 10, 5.
- [12] K. Bian, H. Schunk, D. Ye, A. Hwang, T. S. Luk, R. Li, Z. Wang, H. Fan, *Nat. Commun.* **2018**, 9, 2365.
- [13] N. S. Mueller, E. Pfitzner, Y. Okamura, G. Gordeev, P. Kusch, H. Lange, J. Heberle, F. Schulz, S. Reich, *ACS Nano* **2021**, 15, 5523.
- [14] I. H. Lee, D. Yoo, P. Avouris, T. Low, S. H. Oh, *Nat. Nanotechnol.* **2019**, 14, 313.
- [15] P. T. Bowen, A. Baron, D. R. Smith, *Phys. Rev. A* **2016**, 93, 063849.
- [16] P. C. Wu, C. G. Khoury, T. H. Kim, Y. Yang, M. Losurdo, G. V. Bianco, T. Vo-Dinh,A. S. Brown, H. O. Everitt, *J. Am. Chem. Soc.* 2009, 131, 12032.
- [17] A. G. Marin, T. Garcia-Mendiola, C. N. Bernabeu, M. J. Hernandez, J. Piqueras, J. L. Pau, F. Pariente, E. Lorenzo, *Nanoscale* **2016**, 8, 9842.
- [18] M. G. Blaber, C. J. Engel, S. R. Vivekchand, S. M. Lubin, T. W. Odom, G. C. Schatz, Nano Lett. 2012, 12, 5275.
- [19] M. W. Knight, T. Coenen, Y. Yang, B. J. Brenny, M. Losurdo, A. S. Brown, H. O. Everitt, A. Polman, *ACS Nano* **2015**, 9, 2049.
- [20] A. Bhardwaj, S. Singh Verma, *Biomed. Sci.* **2019**, 5, 27.
- [21] J. Wang, S. Liu, A. Nahata, *Opt. Express* **2012**, 20, 12119.
- [22] J. Wang, S. Liu, Z. V. Vardeny, A. Nahata, Opt. Express 2012, 20, 2346.

- [23] Q. H. Song, W. M. Zhu, P. C. Wu, W. Zhang, Q. Y. S. Wu, J. H. Teng, Z. X. Shen, P.
   H. J. Chong, Q. X. Liang, Z. C. Yang, D. P. Tsai, T. Bourouina, Y. Leprince-Wang, A. Q.
   Liu, APL Mater. 2017, 5, 151105.
- [24] R. Adato, A. A. Yanik, J. J. Amsden, D. L. Kaplan, F. G. Omenetto, M. K. Hong, S. Erramilli, H. Altug, *Proc. Natl. Acad. Sci. U.S.A.* **2009**, 106, 19227.
- [25] D. Rodrigo, O. Limaj, D. Janner, D. Etezadi, F. J. Garcia de Abajo, V. Pruneri, H. Altug, *Science* **2015**, 349, 165.
- [26] A. Di Cicco, Phys. Rev. Lett. 1998, 81, 2942.
- [27] X. Chen, C. Wang, Y. Yao, C. Wang, ACS Nano 2017, 11, 8034.
- [28] P. H. Eilers, Anal. Chem. **2003**, 75, 3631.
- [29] F. Neubrech, A. Pucci, T. W. Cornelius, S. Karim, A. Garcia-Etxarri, J. Aizpurua, *Phys. Rev. Lett.* **2008**, 101, 157403.
- [30] C. Huck, A. Toma, F. Neubrech, M. Chirumamilla, J. Vogt, F. De Angelis, A. Pucci, *ACS Photonics* **2015**, 2, 497.
- [31] D. Ji, A. Cheney, N. Zhang, H. Song, J. Gao, X. Zeng, H. Hu, S. Jiang, Z. Yu, Q. Gan, *Adv. Opt. Mater.* **2017**, 5, 17700233.
- [32] R. Adato, A. Artar, S. Erramilli, H. Altug, *Nano Lett.* **2013**, 13, 2584.
- [33] S. C. Hardy, J. Cryst. Growth 1985, 71, 602.
- [34] Y. Luo, A. I. Fernandez-Dominguez, A. Wiener, S. A. Maier, J. B. Pendry, *Phys. Rev. Lett.* **2013**, 111, 093901.
- [35] P. Nagpal, N. C. Lindquist, S.-H. Oh, D. J. Norris, Science 2009, 325, 594.
- [36] E. D. Palik, Handbook of Optical Constants of Solids, Academic Press, 1998.
- [37] J. C. Love, L. A. Estroff, J. K. Kriebel, R. G. Nuzzo, G. M. Whitesides, *Chem. Rev.* **2005**, 105, 1103.

Xianglong Miao, Ting Shan Luk and Peter Q. Liu\*

#### Liquid-Metal-Based Nanophotonic Structures for High-Performance SEIRA Sensing

#### ToC Figure



A new type of high-performance nanophotonic SEIRA sensors, which utilizes liquid gallium not only as the metallic ground plane of nano-patch antennas but also to sandwich thin analyte films in the nanometric gaps of the nano-patch antennas, is reported. Superior performances for sensing monolayer 1-octadecanethiol and thin PMMA films are achieved. A straightforward and cost-effective procedure for realizing such liquid-gallium-based nanophotonic sensors is developed, which is suitable for point-of-care applications.